

HierRelTriple: Guiding Indoor Layout Generation with Hierarchical Relationship Triplet Losses

Kaifan Sun, Bingchen Yang, Peter Wonka, Jun Xiao, Haiyong Jiang

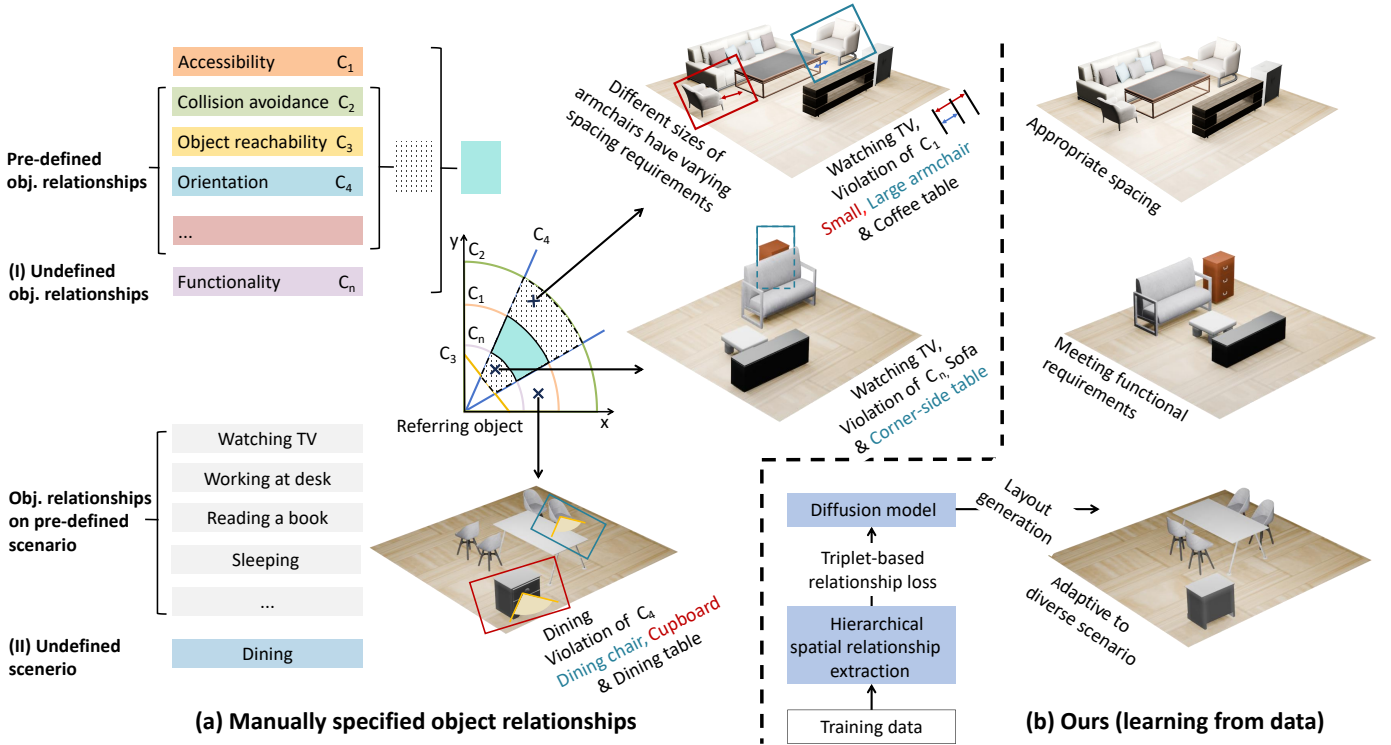


Fig. 1: Comparison of indoor layout synthesis methods: (a) Manually specified relationships tend to be incomplete, resulting in unrealistic layout generation. (b) Our data-driven relationship learning derives important spatial relationships automatically from the dataset, enabling the creation of well-organized layouts.

Abstract—We present a hierarchical triplet-based indoor relationship learning method, coined HierRelTriple, with a focus on spatial relationship learning. Existing approaches often depend on manually defined spatial rules or simplified pairwise representations, which fail to capture complex, multi-object relationships found in real scenarios and lead to overcrowded or physically implausible arrangements. We introduce HierRelTriple, a hierarchical relational triplets modeling framework that first partitions functional regions and then automatically extracts three levels of spatial relationships: object-to-region (O2R), object-to-object (O2O), and corner-to-corner (C2C). By representing these relationships as geometric triplets and employing approaches based on Delaunay Triangulation to establish spatial priors, we derive IoU loss between denoised and ground truth triplets and integrate them seamlessly into the diffusion denoising process. The introduction of the joint formulation of inter-object dis-

tances, angular orientations, and spatial relationships enhances the physical realism of the generated scenes. Extensive experiments on unconditional layout synthesis, floorplan-conditioned layout generation, and scene rearrangement demonstrate that HierRelTriple improves spatial-relation metrics by over 15% and substantially reduces collisions and boundary violations compared to state-of-the-art methods.

Index Terms—Layout Generation, Indoor Scene, Spatial Relationships, and Differentiable Rendering.

I. INTRODUCTION

Automatically generating indoor layouts is critical for a range of applications, including virtual and augmented reality (VR/AR) [1], smart home systems [2], robotics [3], and interior designs [4]–[6]. The rise of generative models [7]–[10] has unlocked new possibilities, significantly advancing both quality and efficiency of indoor layout generation. Despite the progress, generating layouts with practical usability and proper spacing relationships among objects and floorplan boundaries remains an open challenge. Achieving this goal requires a

Kaifan Sun, Bingchen Yang, Jun Xiao, and Haiyong Jiang are with the University of Chinese Academy of Sciences (UCAS), Beijing 100049, China (e-mail: {sunkaifan22, yangbingchen211}@mailsucas.ac.cn, {xiaojun, haiyong.jiang}@ucas.ac.cn). Peter Wonka is with the King Abdullah University of Science and Technology (KAUST), Thuwal 23955, Saudi Arabia (e-mail: pwonka@gmail.com). Haiyong is the Project Lead.

Kaifan Sun and Bingchen Yang contributed equally.

Haiyong Jiang and Jun Xiao are the corresponding authors.

compilation of physical constraints, ergonomic rules, walking spacing, co-occurring object placements, and so on.

Recent approaches [11]–[15] derive primary object relationships from expert knowledge to aid layout generation, such as collision avoidance [11], [12], object reachability [12], [14], and human behavior guidance [13], [15]. These relationships are constructed and enforced as additional regularizations [11], [14] and classifier guidance on a generative model [12]. However, most methods focus on specific relationships based on predefined rules and parameters and usually do not consider the proper spacing between objects and an object to a functional region. For example, PhyScene [12] emphasizes collision avoidance and reachability, but there is no regularization to maintain object spacing between functionally related objects. Forest2Seq [16] establishes hierarchical object relationships but provides insufficient modeling of the relative relationships among sibling objects. As shown in Fig. 1 (a), armchairs of different sizes impose distinct spacing requirements. A sofa can be positioned too close to the corner-side table while being far from the coffee table and TV stand. Another work, LayoutEnhancer [14], lacks spacing relations to floorplan boundaries and functional regions, leading to boundary violations between objects and the wall. Moreover, category-wise relationship modeling, e.g., LayoutEnhancer, requires tedious manual efforts to determine affected objects by each relationship type and is not scalable.

In light of these problems, we directly learn object spacings from the training data as illustrated in Fig. 1 (b). The spacing between nearby objects within a functional region is usually important to ensure functional pathways and physical interactivity. In addition, the spacing between an object and the functional region bounds can avoid boundary violations and unreasonable object positions. To facilitate automatic relationship extraction, we observe that the three-level hierarchy, i.e., furniture-functional region-layout, can partition objects within a layout and that the geometric properties of the Delaunay Triangulation (DT) facilitate grouping proximate object triplets as a DT triangle, and emphasizing objects with a larger shape size with DT weights during relationship learning.

From another perspective, previous works [11], [12], [14] mainly model pairwise relationships between two objects, making it difficult to account for high-order object interactions and important indoor design principles. A typical example is the kitchen work triangle [17] that addresses the efficiency between major work centers, including cooking, sink, and refrigerator. Similar examples can be found in a living room, e.g., the triangular layout among sofa, armchairs, and TVs. Therefore, introducing high-order triplet-based relationships can consider interactions among three objects and constrain relative positions better.

We propose a novel framework, HierRelTriple, to render the two above-mentioned observations to integrate spatial relationships into a generative model. The overall pipeline of HierRelTriple is shown in Fig. 2 and is based on Dif-fuScene [18]. First, we automatically extract important relationships from an input layout hierarchically for training. The relationship extraction begins by grouping nearby objects into functional regions. We categorize spatial relationships into

three types, including relative placement of an object with respect to its belonging functional region, the spacing between the centroids of two objects within a functional region, and nearby relationships between corners of any two objects. We further subdivide these relationships into a set of triplets using DT. Thereafter, we present a unified framework that enforces triplet-based relationships with an IoU loss. The diffusion process is optimized using both the diffusion loss and the proposed losses for relationship learning. The source code and trained models will be released. Our main contributions are as follows.

- 1) A method to automatically extract important object-to-region, object-to-object, and corner-to-corner relationships as triplets from an input floorplan.
- 2) An IoU-based loss for the learning of triplet relationships during the training of a diffusion model.
- 3) Superior performance on established scene synthesis metrics and significant improvements (at least 15%) over existing methods on newly introduced spatial relationship metrics for three tasks.

II. RELATED WORK

In this section, we first review generative indoor layout modelling methods, including approaches based on VAEs, GANs, autoregressive models, and diffusion. We then discuss graph-based relationship learning methods that capture high-level spatial and semantic dependencies. Finally, we examine optimisation-based strategies for integrating fine-grained functional and geometric constraints into layout generation.

A. Generative Indoor Layout Modeling

The success of generative models in image generations [19], [20] has encouraged likewise explorations in indoor layout modelling, including variational autoencoder (VAE)-based methods [21]–[23], GAN-based methods [24]–[27], autoregressive models [7], [8], [28]–[32], and diffusion models [9], [11], [12], [33]–[35]. Another interesting trend [36]–[42] is to leverage autoregressive Large Language Models (LLMs) as visual scene planners, generating layouts as structured text programs. Some interesting works [9], [11], [12], [34] explore diffusion models for layout rearrangement and conditional and unconditional indoor layout modelling. While these diverse generative approaches have demonstrated significant capabilities in synthesising plausible furniture arrangements, their primary focus often lies in generating sets of objects with plausible categorical and geometric attributes (e.g., type, size, position) within a scene. However, explicit and structured modelling of the spatial relationships between objects remains a less emphasised or implicitly learnt aspect in many existing frameworks. Compared to the methods above, this work focuses on modelling spatial relationships with inter-object functional requirements.

B. Graph-based Relationship Learning for Indoor Layouts

Plausible indoor layouts are usually bound with complex layout relationships [43], such as co-occurrence, functionality,

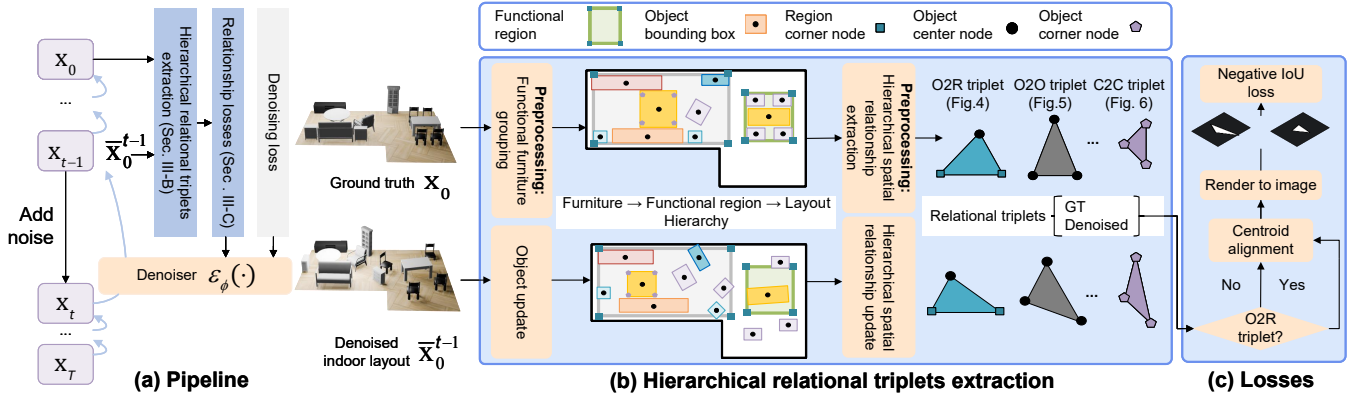


Fig. 2: Overview of HierRelTriple. (a) Spatial relationships are automatically extracted and modeled, then integrated into diffusion-based model training through a rendering loss. (b) A hierarchical approach is applied to identify important spatial relationships. (c) Evaluation of these losses is performed through differentiable rendering.

feasible placement, and layout balance. One line of work abstracts layout relationships as a graph for graph-preconditioned layout modelling. The relationship graph can be manually specified [21], [23], [34], [44]–[46] or generated [22], [29], [30], [33], [47]–[50], with nodes representing furniture objects annotated with attributes and edges encoding targeted spatial and semantic relationships (e.g., orientation, functional grouping). However, while effectively propagating high-level relational semantics and topological structures, these methods often lack explicit mechanisms to satisfy fine-grained, geometric constraints inherent in spatial relationships. Generated geometries (e.g., positions, orientations) may statistically approximate relational priors learnt from data, but critical functional constraints (e.g., maintaining minimal clearance distances or strictly avoiding object interpenetration) are missed. Compared to these graph-conditioned approaches, our work learns relationships with hierarchically constructed relationship losses and the diffusion process.

C. Optimization-based Indoor Relationship Integration

Spatial relationships are crucial for physically and functionally plausible indoor layouts. The core challenge lies in effectively integrating these relationships into the optimization process. A common strategy involves optimizing a density function using Markov Chain Monte Carlo (MCMC) [51]–[53] or position-based dynamics [54]–[56], which enable satisfying fundamental constraints like collision avoidance and containment within boundaries.

Another scheme incorporates additional relationships by deep reinforcement learning [13] and additional conditional guidance on deep generative models. PhyScene [12] and SHADE [57] adopt the classifier-guidance diffusion model [18] to optimize indoor layouts with collision avoidance and object reachability. Ergonomic rules and human interaction constraints have been formulated as differentiable objective functions that are optimized directly within the training loop of generative models [14], targeting functional aspects like human movement paths and interaction.

Compared to these relation-wise formulations, which often require specialized handling for each constraint type (e.g., sep-

arate collision functions [11], [12], reachability metrics [12], [14], or path planning objectives [13]), our approach encodes diverse object relationships using a unified triple representation, which is easily integrated with rendering-based loss functions for efficient joint optimization.

III. METHOD

Our goal is to learn a generative model that can generate indoor layouts with plausible object relationships. The overall pipeline is illustrated in Fig. 2. We start by introducing the layout representation and the layout diffusion model in Sec. III-A. To further learn indoor spatial relationships, we proceed to build three categories of relational triplets using the training data (see Sec. III-B). These include mutual relationships linking objects to their respective functional regions, relationships between distinct objects, and relationships between object corners. We enforce these relationships using differentiable rendering-based losses and train the diffusion model by combining it with the diffusion loss (see Sec. III-C). During inference, our method directly generates an indoor layout via the diffusion model without reliance on the spatial relationship construction.

A. The Layout Diffusion Model

We encode an indoor layout as $\mathbf{x} = \{o_1, o_2, \dots, o_N\}$ with N objects, where N varies for different layouts. Each object o_i has a set of parameters $o_i = \{c_i, b_i, f_i\}$, where $c_i \in \mathbb{R}^C$ indicates its category within a set of C categories. $b_i = (s_i, p_i, r_i)$ is the 3D bounding box of the object o_i , defined by its size $s_i \in \mathbb{R}^3$, the coordinate of centroid $p_i \in \mathbb{R}^3$, and the ground plane orientation $r_i = (\cos \theta_i, \sin \theta_i) \in \mathbb{R}^2$. $f_i \in \mathbb{R}^{32}$ denotes a 3D object feature encoding the shape of the object and can be used for furniture retrieval.

Our method is built based on DiffuScene [11] and can easily incorporate other indoor layout generative models, e.g., autoregressive model-based ATISS. Starting with a clean indoor layout $\mathbf{x}_0 = \mathbf{x}$, we gradually add Gaussian noise through a forward diffusion process, transforming \mathbf{x}_0 into noisy data

\mathbf{x}_T . This forward process consists of a series of transitions $q(\mathbf{x}_t | \mathbf{x}_{t-1})$ as follows:

$$q(\mathbf{x}_t | \mathbf{x}_{t-1}) = \mathcal{N}(\mathbf{x}_t; \sqrt{\alpha_t}\mathbf{x}_{t-1}, (1 - \alpha_t)\mathbf{I}) \quad (1)$$

β_t controls the noise variance at each time step. During the generative process, we gradually denoise noisy layout $\mathbf{x}_T \sim \mathcal{N}(0, \mathbf{I})$ with the reverse process $p(\mathbf{x}_{t-1} | \mathbf{x}_t)$. The reverse process is optimized by maximizing the log-likelihood of $p(\mathbf{x}_0)$:

$$\mathcal{L}_{\text{diff}} = \mathbb{E}_{\mathbf{x}_0, \epsilon, t} [\|\epsilon - \epsilon_\phi(\mathbf{x}_t, t)\|_2^2], \quad (2)$$

where ϵ denotes the added Gaussian noise in each step, and $\epsilon_\phi(\mathbf{x}_t, t)$ is a denoising network. The denoising network $\epsilon_\phi(\mathbf{x}_t, t)$ adopts a UNet-1D module with self-attention [58].

During training, although the denoising model predicts the noise $\epsilon_\phi(\mathbf{x}_t, t)$ at time step t , we can deterministically (without iterative sampling) recover the denoised layout $\bar{\mathbf{x}}_0^t$ (an estimate of the ground-truth \mathbf{x}_0) from Eq. 3 as,

$$\bar{\mathbf{x}}_0^t = \frac{1}{\sqrt{\bar{\alpha}_t}} (\mathbf{x}_t - \sqrt{1 - \bar{\alpha}_t} \epsilon_\phi(\mathbf{x}_t, t)) \quad (3)$$

where $\bar{\alpha}_t = \prod_{i=1}^t \alpha_i$. This denoised layout will enable us to compute the relationship losses in Sec. III-C.

B. Hierarchical Relational Triplets Extraction

Indoor spatial relationships, e.g., walking space maintenance, collision avoidance, and co-occurrence between nearby objects, are usually organized hierarchically, following the object-functional region-layout hierarchy of indoor scenes as illustrated in Fig. 2 (b). For example, a sofa and a corner table in the living room need to maintain appropriate spacing to accommodate proper interactions between the table and the human on the sofa, while subdivided regions within the layout restrict the spatial boundaries of objects, such as a dining table within the dining region. To extract hierarchical spatial relationships, we first extract functional regions to construct a three-level indoor hierarchy and then divide spatial relationships into three types. This process can be done as a one-time preprocessing step for each input layout and is only executed for the training stage.

To construct functional regions, we project the indoor layout onto the ground plane and represent objects as vertices. We group objects as functional regions using clustering and encode functional regions as rectangles. Following SceneHGN [22], we utilize DBSCAN [59] to delineate object clusters based on the overlapping ratio and the distance criteria between any two objects o_i, o_j :

$$m_{ij} = d_{ij} + \lambda_{\text{giou}} \cdot (1 - \text{GIoU}(b_i, b_j)), \quad (4)$$

where $\text{GIoU}(\cdot) \in [-1, 1]$ [60] takes into account the influence of bounding boxes b_i, b_j of two objects and $d_{ij} = \|p_i - p_j\|_{xy}^2$ is the Euclidean distance between the centroids of the two objects on the ground plane. We define the functional regions as the bounding box of each cluster. The vertex coordinates of each region are derived from the maximum-minimum operator applied on the centroid coordinates of all objects within the cluster. Fig. 3 shows some constructed functional regions.

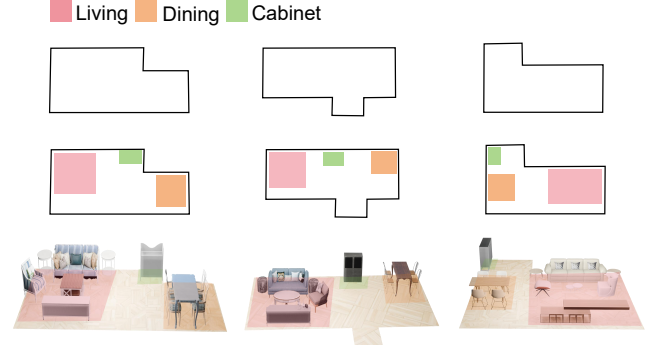


Fig. 3: Three functional regions (Living, Dining, and Cabinet) are identified within the scene through color-based delineation.

After obtaining the functional regions, we then extract hierarchical spatial relationships. Previous arts [12]–[14] optimize indoor relationships according to different formulations of semantics and functionality, such as collision avoidance, walking space, and functional relevance. These formulations predominantly boil down to optimizing spatial distances between objects. Our approach diverges by optimizing spatial relationships according to their relevance within the indoor hierarchy. For example, collision avoidance mainly constrains the relative distance between object corners, while functionally related objects usually follow specific spatial patterns between object positions. We build three types of spatial relationships: object-to-functional region (O2R) relationships that encode the spatial relationship between individual objects and layout regions, object-to-object (O2O) relationships that encode relative distances among the centroids of objects, and corner-to-corner (C2C) relationships that restrict distances between two objects’ corners.

O2R Triplets. O2R relationships model the relative spatial distribution of a specific object concerning its belonging functional region. We treat the four corners of a functional region, determined by its bounding box, as virtual nodes. The furniture object with the largest size, which is usually the dominant object of a functional region, is then connected to these four virtual nodes of its associated functional region, forming four triangles. These triangles, each composed of one real furniture object and two virtual corner points, constitute the O2R triplets. We filter out elongated triangles containing any interior angle exceeding 160° . A sample illustrating the construction of O2R triples is shown in Fig. 4. These triplets serve as a fundamental mechanism to explicitly model the critical spatial relationships that must be maintained between furniture items and the boundaries of their designated functional regions within the room. This modeling encompasses essential constraints such as ensuring furniture avoids breaching room or region boundaries, thereby maintaining safe and practical clearances. It also includes guiding the placement of key, dominant objects, exemplified by a bed in a bedroom or a sofa in a living room, into the central area of their respective regions to establish visual balance and functional prominence.

O2O Triplets. Each functional region usually has a functionally dominant object, e.g., a bed in a bedroom, and most

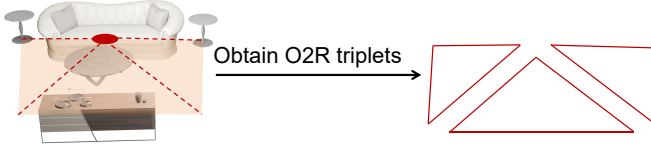


Fig. 4: An example illustrating the construction of an O2R triplet.

other objects are affected by the position of the dominant object, e.g., chairs surrounding a dining table. Meanwhile, the proximity compatibility principle [61] suggests that spatially close objects are more likely to be related. To fulfil these two criteria, we employ Weighted Delaunay Triangulation (WDT) [62] to partition object relationships into O2O triples with each object as a WDT point. As an object with larger occupancies is usually more important in a functional region, we calculate the WDT weight for each object using the multiplication of its size. Compared to Delaunay Triangulation (DT), WDT places more emphasis on larger objects and generates denser connections for large objects, as illustrated in Fig. 5. However, when two furniture objects exhibit significant weight disparity, WDT may fail to connect some points despite geometric proximity. Approximately 5% of living rooms encountered such unconnected points. To resolve this, we iterate through each triangle generated by the weighted Delaunay triangulation and link unconnected points and triangle points formed by WDT by performing DT inside each triangle with unconnected points, ensuring connectivity for all objects. If the region contains only two objects, we introduce an additional virtual node to construct an equilateral triplet. A comparative illustration of DT, WDT, and our approach is presented in Fig. 5. Therefore, O2O relationships are converted to a set of O2O triplets among objects.

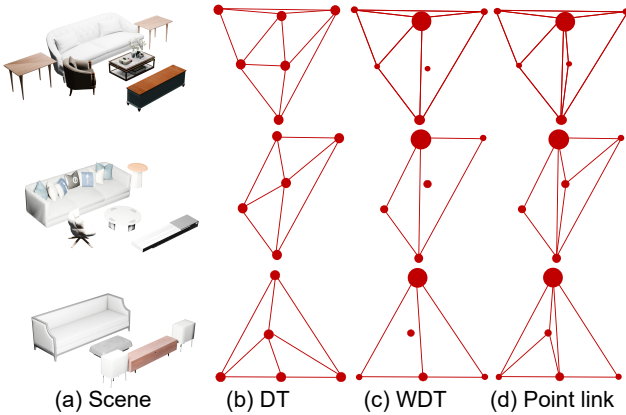


Fig. 5: The comparison of the construction of O2O triplets using DT (b), WDT (c), and our PointLink (d) for input scenes (a).

C2C Triplets. As O2O triplets represent each object as a point and ignore fine-grained spatial relationships between the bounding boxes of two objects. We further introduce C2C triplets to account for this type of relationship. Fig. 6 illustrates an example of constructing a C2C triplet. The minimum convex polygon formed by the vertices of three non-overlapping

furniture bounding boxes is defined as the outer ring (shown in red in Fig. 6), while the remaining vertices constitute the inner ring (shown in blue in Fig. 6). We tessellate the space between the inner ring and the outer ring with Constrained Delaunay Triangulation (CDT) [63]. The tessellated triangles formed by the corners of any two objects mark the relative spatial positions between two objects. The input to CDT is a planar straight-line graph with all corners as input vertices and the edges of object-triplet bounding boxes, the inner ring, and the outer ring as input line segments. We filter the resulting tessellated triangles that are within any bounding boxes and inner loops as the C2C triplets. These C2C triplets characterize the relative spatial positions between object corners.

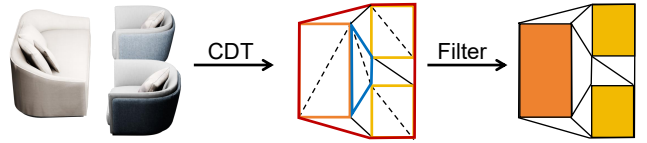


Fig. 6: An example of the C2C triplet construction.

The relational triplets, including those derived from DBSCAN-based functional region grouping and DT methods, are precomputed for each training data and remain unchanged during training, regardless of the positions of their constituent objects perturbed by the noise injection. Therefore, they do not introduce additional computational overhead for the model training and have no impact on the denoising speed when performing as relational supervision as described in Sec. III-C.

C. Relationship Losses

To encourage the layout diffusion model to capture hierarchical spatial relationships, we introduce relationship losses on the denoised layout \bar{x}_0^t during the training phase, namely \mathcal{L}_{O2R} , \mathcal{L}_{O2O} , \mathcal{L}_{C2C} , by measuring discrepancies between ground-truth O2R, O2O and C2C triplets and their denoised counterparts. An intuitive approach is to supervise the geometric attributes of the triangles formed by relational triplets, which helps preserve their internal structure. However, supervising multiple geometric attributes simultaneously is nontrivial, as their relative significance often shifts across different layouts and makes it difficult to strike a balance. Besides, we observe that a triplet is only functionally plausible when placed in an appropriate region of the layout. For example, arbitrarily rotating an O2O triplet composed of a sofa and two corner-side tables in a living region, though not offending its internal geometry, can undermine the global layout not only due to this triplet being misaligned with the designated orientation, but also because it interferes with spatial relationships involved by other triplets.

To this end, we expect a spatial-aware relationship loss that can effectively penalize spatial misalignment, while also offering a holistic perspective for capturing diverse geometric variations among triplets. We intuitively employ a negative IoU loss. In order to avoid the instability of calculating triangles' intersection and for implementation convenience, we

adopt differentiable rasterization of triangles and estimate IoU at the pixel level. The loss \mathcal{L}_{O2R} can be calculated as Eq. 5:

$$\mathcal{L}_{O2R} = 1 - \frac{1}{|\overline{M}_{O2R}|} \cdot \sum_{\substack{\overline{m}_i \in \overline{M}_{O2R}, \\ m_i \in M_{O2R}}} \mathbf{IoU}(\mathcal{R}(\overline{m}_i), \mathcal{R}(m_i)), \quad (5)$$

where $\mathcal{R}(\cdot)$ denotes differentiable rendering taking a triangle as input, $|\overline{M}_{O2R}|$ denotes the number of O2R triplets within the denoised layout $\overline{\mathbf{x}}_0^t$, and $\mathbf{IoU}(\cdot, \cdot)$ computes the IoU between triangles formed by prediction and ground-truth triplets.

The O2O and C2C losses \mathcal{L}_{O2O} , \mathcal{L}_{C2C} are computed using a similar formulation but with a slight modification: we align the centroids of the denoised and ground-truth triplets before computing the IoU. This alignment ensures that the losses focus on structural differences in the triangle’s shape and orientation, rather than being dominated by absolute spatial displacement. In doing so, the loss better captures geometric discrepancies while remaining invariant to global translation.

The overall optimization objective is a summation $\mathcal{L} = \mathcal{L}_{\text{diff}} + \lambda_{O2R} \cdot \mathcal{L}_{O2R} + \lambda_{O2O} \cdot \mathcal{L}_{O2O} + \lambda_{C2C} \cdot \mathcal{L}_{C2C}$ with balancing weights λ_{O2R} , λ_{O2O} and λ_{C2C} .

IV. EXPERIMENTS AND RESULTS

In this section, we evaluate the method on three tasks, including unconditional indoor layout generation, floorplan-conditioned indoor layout generation, and indoor layout rearrangement. After that, we ablate key components and hyperparameters.

A. Experimental Settings

Datasets. We use the 3D-FRONT dataset [64] for experiments. Following previous work [11], [12], we select a subset of rooms containing 4,041 bedrooms, 900 dining rooms, and 813 living rooms. For each room category, 80% of the rooms are used for training, while the remaining 20% are reserved for testing.

Metrics. To evaluate the visual quality of generated scenes, we follow Diffuscene [11] and employ perceptual similarity Fréchet Inception Distance (FID) [65], Kernel Inception Distance (KID $\times 0.001$) [66], Scene Classification Accuracy (SCA), and categorical KL Divergence (CKL $\times 0.01$). FID, KID, and SCA are highly sensitive to shape textures and rendering styles. To ensure fairness, we render the results of all competing methods using the same configuration. Following PhyScene [12], we adopt Col_{obj} , $\text{Col}_{\text{scene}}$, and R_{out} to assess the violation of important spatial relationships. Col_{obj} represents the percentage of objects that collide with others, and $\text{Col}_{\text{scene}}$ denotes the percentage of generated layouts where the object collision occurs. R_{out} evaluates the proportion of objects that extend beyond the floorplan in the floor-conditioned layout synthesis. For Col_{obj} , $\text{Col}_{\text{scene}}$, R_{out} , lower values are better.

We additionally introduce a metric D_{obj} to measure the changes in spatial distance distribution between frequently co-occurring object pairs in synthesised layouts and ground truth. A furniture pair is frequent if it appears more than a specified portion (50% in our experiments). For all furniture pairs with specific semantics in the training set, we compute

TABLE I: Statistics of relative Euclidean distances between furniture pairs.

Room	Furniture Pair	Average Distance
Dining room	cabinet - dining_chair	0.524
	dining_chair - dining_table	0.176
	corner_side_table - dining_table	0.745
	coffee_table - dining_table	0.689
	coffee_table - corner_side_table	0.397
	console_table - dining_chair	0.475
	dining_chair - dining_chair	0.244
	dining_chair - multi_seat_sofa	0.734
	armchair - dining_chair	0.832
	coffee_table - dining_chair	0.720
	dining_chair - tv_stand	0.779
	coffee_table - tv_stand	0.371
	dining_chair - loveseat_sofa	0.795
	corner_side_table - dining_chair	0.774
bookshelf - dining_chair	0.541	
dining_chair - wine_cabinet	0.459	
dining_chair - stool	0.526	
Bedroom	double_bed - wardrobe	0.730
	nightstand - wardrobe	0.882
	double_bed - nightstand	0.571
	nightstand - nightstand	0.907
Living room	coffee_table - multi_seat_sofa	0.256
	corner_side_table - multi_seat_sofa	0.315
	armchair - coffee_table	0.301
	armchair - corner_side_table	0.418
	coffee_table - corner_side_table	0.405
	coffee_table - dining_table	0.689
	dining_chair - dining_table	0.173
	dining_chair - dining_chair	0.231
	dining_chair - loveseat_sofa	0.784
	coffee_table - tv_stand	0.366
	corner_side_table - tv_stand	0.638
	coffee_table - dining_chair	0.719
	dining_table - tv_stand	0.723
	corner_side_table - dining_table	0.735
	dining_chair - tv_stand	0.757
	corner_side_table - dining_chair	0.767
	bookshelf - dining_chair	0.526
	dining_chair - multi_seat_sofa	0.742
	armchair - dining_chair	0.822
	dining_chair - wine_cabinet	0.493
console_table - dining_chair	0.483	
dining_chair - stool	0.571	
cabinet - dining_chair	0.568	
dining_chair - lounge_chair	0.797	

the Euclidean distance between their normalized centroids, and adopt Gaussian kernel density estimation for their distance distribution, with the bandwidth for the kernel selected via Scott’s rule [67]. At last, D_{obj} takes the averaged absolute differences of distance expectations between predicted furniture pairs and ground truth ones as the metric. The distance expectation for all frequent furniture pairs in the ground truth is presented in Tab. I.

Baselines. For indoor layout synthesis, we compare with four state-of-the-art methods: 1) ATISS [8], an autoregressive network for indoor layout generation; 2) LayoutEnhancer [14], an autoregressive model incorporating ergonomic and indoor functional design knowledge as a training regularization term; 3) DiffuScene [11], a DDPM-based indoor layout synthesis model that introduces IoU regularization terms to penalize object collisions; 4) PhyScene [12], which models pairwise object relationships as a binary classifier and provides classifier guidance for a DDPM-based indoor layout synthesis model; and 5) Forest2Seq [16], a method that organizes unordered

TABLE II: Quantitative comparisons on unconditioned layout generation.

Room	Method	FID↓	KID $\times 0.001$ ↓	SCA	CKL $\times 0.01$ ↓	Col $_{obj}$ ↓	Col $_{scene}$ ↓	D $_{obj}$ ↓
Bedroom	ATISS	56.628	4.764	0.542	0.752	0.291	0.546	0.172
	LayoutEnhancer	42.515	4.241	0.523	0.526	0.256	0.488	0.108
	DiffuScene	39.422	4.352	0.527	0.396	0.247	0.462	0.072
	Forest2Seq	38.412	3.925	0.519	0.343	0.238	0.457	0.062
	Ours	27.247	1.281	0.511	0.254	0.212	0.410	0.030
Living room	ATISS	74.522	5.671	0.592	0.511	0.384	0.878	0.672
	LayoutEnhancer	68.462	4.862	0.577	0.518	0.314	0.748	0.613
	DiffuScene	50.699	3.792	0.562	0.234	0.221	0.612	0.432
	Forest2Seq	48.235	1.894	0.529	0.231	0.219	0.589	0.398
	Ours	44.566	0.711	0.496	0.125	0.135	0.449	0.206
Dining room	ATISS	72.433	5.524	0.586	0.653	0.422	0.806	0.581
	LayoutEnhancer	69.125	4.924	0.545	0.529	0.352	0.698	0.492
	DiffuScene	49.658	4.256	0.538	0.231	0.224	0.628	0.423
	Forest2Seq	49.127	2.567	0.531	0.229	0.202	0.572	0.386
	Ours	46.453	2.434	0.509	0.161	0.160	0.530	0.185

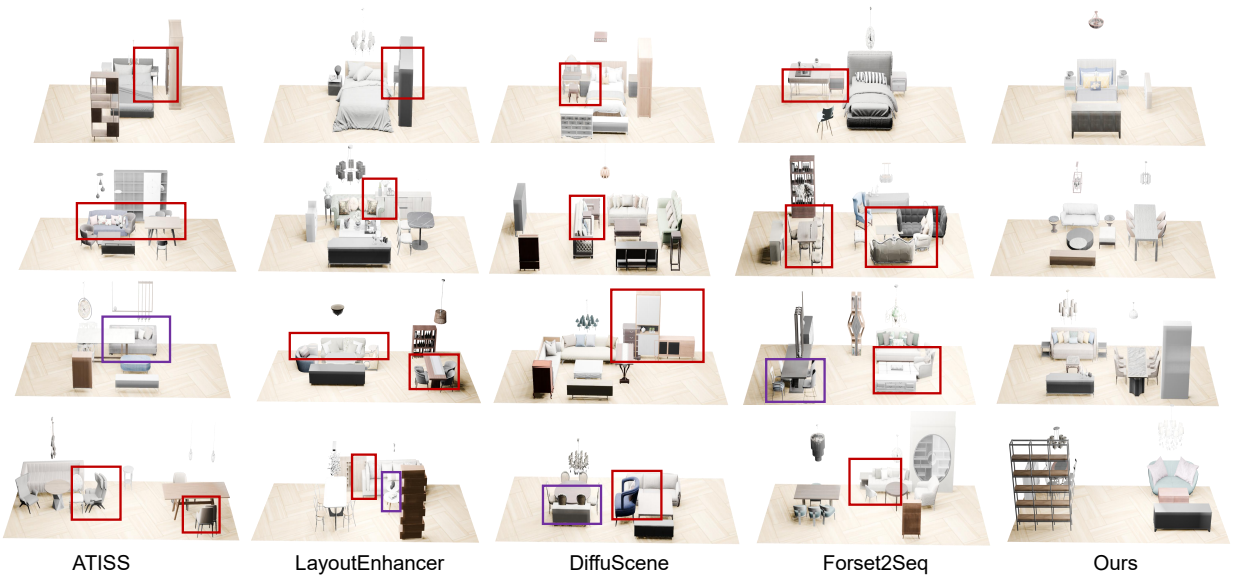


Fig. 7: Qualitative results on unconditional layout synthesis. The red boxes indicate overlaps, while the purple boxes highlight unreasonable furniture distribution.

scene objects into a structured and ordered hierarchical scene tree and forest. Since PhyScene only releases the inference code and the pre-trained model for a floor-conditioned living room. We compare with PhyScene only under this configuration. In addition, we also compare the method with DiffuScene and LEGO [9] for scene rearrangement tasks.

Implementation We train our model using a single NVIDIA A100 GPU, with a batch size of 128, for 100,000 epochs. The initial learning rate was set at 2×10^{-4} and gradually decayed by a factor of 0.5 for every 15,000 epochs. For the diffusion process, we follow the default settings of DDPM [68], where the noise intensity β_t increases linearly from 0.0001 to 0.02 for 1,000 time steps. The complete training for the bedroom, living room, and dining room takes three days. For DBSCAN clustering, epsilon and the min number of samples are set to 1.8 and 2, respectively, with a GIoU weight of $\lambda_{\text{giou}} = 0.02$.

During training, we set the loss weight $\lambda_{\text{O2R}} = 0.025$, $\lambda_{\text{O2O}} = 0.05$, $\lambda_{\text{C2C}} = 0.04$. The output images are rendered with dimensions of 128 pixels by 128 pixels. To evaluate visual metrics FID, KID, and SCA, we construct 3D scenes from the generated indoor layout by retrieving the closest matched CAD furniture from 3D-FUTURE [69] based on the 3D object feature f_i .

B. Unconditioned Indoor Layout Generation

In this scenario, the method directly generates layouts without any input conditions. The quantitative results are presented in Tab. II. HierRelTriple demonstrates a clear advantage across visual quality metrics (FID, KID, SCA, and CKL), showing consistently superior generation quality compared to ATISS, LayoutEnhancer, and DiffuScene. These metrics underscore the effectiveness of incorporating spatial relationships for per-

TABLE III: Quantitative comparisons of floor-conditioned layout synthesis across different methods.

Room	Method	FID↓	KID $\times 0.001$ ↓	SCA	CKL $\times 0.01$ ↓	Col _{obj} ↓	Col _{scene} ↓	D _{obj} ↓	R _{out} ↓
Bedroom	ATISS	50.871	2.264	0.533	0.323	0.278	0.593	0.102	0.302
	LayoutEnhancer	48.984	2.143	0.525	0.299	0.247	0.465	0.082	0.276
	DiffuScene	37.060	2.163	0.528	0.312	0.223	0.434	0.056	0.268
	Forest2Seq	36.102	2.125	0.521	0.268	0.215	0.408	0.049	0.242
	Ours	28.910	1.901	0.516	0.221	0.181	0.329	0.036	0.205
Living room	ATISS	62.920	4.768	0.541	0.212	0.316	0.876	0.771	0.152
	LayoutEnhancer	61.520	4.252	0.535	0.208	0.285	0.874	0.652	0.149
	DiffuScene	49.421	3.546	0.544	0.203	0.254	0.706	0.664	0.248
	PhyScene	50.361	3.632	0.539	0.171	0.202	0.630	0.629	0.220
	Forest2Seq	48.998	2.989	0.538	0.189	0.217	0.654	0.649	0.147
Ours	46.335	1.854	0.514	0.160	0.172	0.499	0.482	0.155	
Dining room	ATISS	65.136	4.762	0.520	0.316	0.415	0.860	0.571	0.146
	LayoutEnhancer	60.106	3.882	0.518	0.298	0.323	0.824	0.480	0.143
	DiffuScene	48.908	2.889	0.517	0.204	0.185	0.586	0.455	0.202
	Forest2Seq	48.312	2.792	0.515	0.191	0.181	0.579	0.428	0.139
	Ours	46.799	2.490	0.510	0.151	0.148	0.479	0.363	0.132



Fig. 8: Visualization comparisons of floor-plan conditioned layout synthesis. The red boxes indicate overlap, the blue boxes indicate out-of-bounds, and the purple boxes highlight areas with unreasonable furniture distribution.

ceptual and semantic accuracy, which is crucial for generating realistic layouts. In terms of collision metrics, HierRelTriple significantly reduces object overlaps and boundary violations. For the living room, HierRelTriple achieves reductions of 38.4% in Col_{obj} and 23.8% in Col_{scene}, relative to Forest2Seq. This improvement indicates effective collision management, suggesting that HierRelTriple is better at collision.

Additionally, HierRelTriple achieves superior performance in D_{obj}, highlighting its ability to maintain consistent distance relationships. In the bedroom layout, for example, HierRelTriple achieves a D_{obj} of 0.030, compared to Forest2Seq (0.062) and DiffuScene (0.072). This reflects HierRelTriple’s precision in preserving relative spacing, contributing to both visual authenticity and physical rationality within generated scenes.

Fig. 7 presents a qualitative comparison of different layout generation methods. Our generated layouts have fewer object collisions, and the object placement is more reasonable, for

example, the proper spacing between a bed and nightstands, a sofa, and its surrounding objects.

C. Floorplan-conditioned Layout Generation

In this scenario, the method generates layouts conditioned on a floorplan input. Tab. III compares HierRelTriple with alternative baselines. Note that PhyScene only provided the pre-trained model and testing code for living room comparisons. Across metrics that assess layout realism and spatial organization, HierRelTriple demonstrates distinct advantages over DiffuScene, LayoutEnhancer, PhyScene, and Forest2Seq. For the living room layout, for example, HierRelTriple achieves a D_{obj} of 0.482, much lower than DiffuScene(0.664) and PhyScene(0.629). This lower D_{obj} value indicates HierRelTriple’s superior control over object distances, effectively maintaining realistic spacing that contributes to both visual coherence and physical plausibility in the layout.

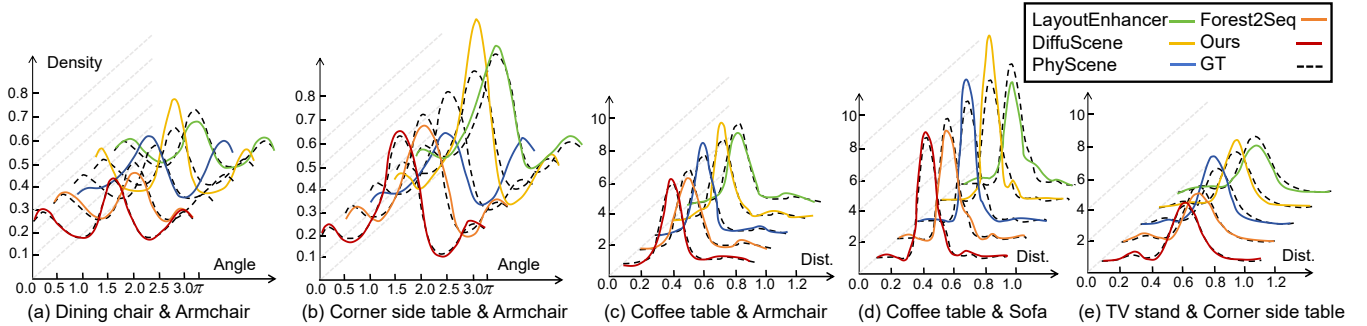


Fig. 9: Distribution of the relative distances and angles between object pairs modeled by five approaches—LayoutEnhancer, DiffuScene, PhyScene, Forest2Seq, and Ours—compared to the ground truth, where (a)-(b) visualizes the angle distribution and (c)-(e) visualizes the distance distribution.

HierRelTriple’s R_{out} is marginally higher than Forest2Seq. A possible reason is that HierRelTriple emphasizes the relationship between objects and regions rather than room boundaries, leading to higher R_{out} but significant improvements in D_{obj} , Col_{obj} , and $\text{Col}_{\text{scene}}$ metrics. Fig. 8 illustrates a visual comparison between various layout synthesis methods. In Fig. 9, we provide a kernel density estimate (KDE) plot of the distance distribution between co-occurring furniture pairs. We can see our method is much closer to the ground truth distribution at the highest density peak and can accurately track the trends of the overall density changes. Therefore, the generated layouts exhibit more similar distance distributions to the ground truth layouts than other methods. Our method produces fewer object obstructions and has less unoccupied space than Forest2Seq and PhyScene.

D. Indoor Layout Re-arrangement

In this task, we take a set of semantic objects and generate an indoor layout for the living room setting. Tab. IV presents the results. We can see the inclusion of HierRelTriple can greatly improve the performance of both baselines and achieve better numbers on all metrics, especially for constraint metrics (see improvements in Col_{obj} , $\text{Col}_{\text{scene}}$, and D_{obj}). Qualitative results in Fig. 10 show superior performance in avoiding object collisions. The integration of HierRelTriple leads to more realistic and functional indoor layouts by enhancing constraint satisfaction.

TABLE IV: Quantitative comparisons on the task of scene arrangement in the 3D-FRONT living rooms. We evaluate results with LEGO and DiffuScene as baseline methods.

Method	FID↓	KID $\times 0.001$ ↓	SCA	Col_{obj} ↓	$\text{Col}_{\text{scene}}$ ↓	D_{obj} ↓
LEGO	66.952	7.592	0.592	0.557	0.898	0.725
Ours(LEGO)	54.912	3.377	0.567	0.386	0.796	0.312
Diffuscene	61.017	5.842	0.586	0.497	0.920	0.495
Ours(Diffuscene)	52.689	2.796	0.559	0.298	0.687	0.278

E. Ablation Studies

In this section, we first evaluate the impact of different triangulation methods on the O2O component. Next, we assess

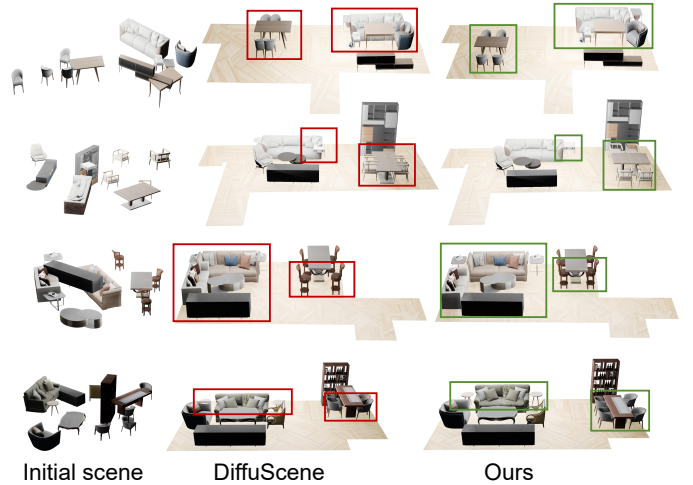


Fig. 10: Visual comparisons on scene re-arrangements where the indoor objects are given. The red boxes mark incorrect furniture placements, while the green boxes indicate appropriate arrangements.

the effectiveness of the three proposed loss functions. Finally, we compare our method with four alternative rendering loss designs. All experiments are conducted for unconditional living room generation.

Alternatives for O2O Triplet Construction. We compared the impact of different triangulation methods: selecting two nearest neighbors for each object as O2O triplets (2NN), replacing WDT with DT, WDT, and our WDT with point links on the generated results. The results presented in Tab. VI demonstrate that WDT with point links yields the best performance, indicating O2O triplets constructed with an emphasis on object sizes can effectively identify important relationships.

Impact of O2R, O2O, and C2C Losses. In Tab. VII, we explore how O2R and O2O losses affect the generation quality. We evaluate the results of the unconditional generation in living rooms. The O2R loss focuses on fitting objects within designated regions of the indoor layout, ensuring that each object is placed appropriately within the layout. Comparing row 1 and row 2, the generated indoor layout also achieves significant improvements in Col_{obj} ($0.254 \rightarrow 0.168$),

TABLE V: Analysis of alternative spatial relationship modeling strategies.

spt. relationship	reg. term	FID↓	KID $\times 0.001$ ↓	SCA	CKL $\times 0.01$ ↓	Col _{obj} ↓	Col _{scene} ↓	D _{obj} ↓
pairwise	–	46.184	1.026	0.516	0.226	0.191	0.569	0.400
triplet	MSE-based loss	45.860	0.950	0.511	0.189	0.142	0.510	0.217
	IoU-based loss	44.566	0.711	0.496	0.125	0.135	0.449	0.206

TABLE VI: Ablation study on triangulation methods for O2O.

Method	FID↓	KID $\times 0.001$ ↓	SCA	CKL $\times 0.01$ ↓	Col _{obj} ↓	Col _{scene} ↓	D _{obj} ↓
2NN	46.962	1.124	0.521	0.212	0.154	0.532	0.352
DT	45.860	0.950	0.511	0.189	0.142	0.510	0.217
WDT	44.912	0.836	0.507	0.138	0.139	0.460	0.211
Point links	44.566	0.711	0.496	0.125	0.135	0.449	0.206

Col_{scene} (0.762 \rightarrow 0.555), and D_{obj} (0.452 \rightarrow 0.292). Comparing row 1 and row 3 in Tab. VII, the O2O loss plays a crucial role in managing important spatial relationships (Col_{obj} 0.254 \rightarrow 0.140, Col_{scene} 0.762 \rightarrow 0.460), and shows better distribution of object spacing (D_{obj} 0.452 \rightarrow 0.218), indicating the avoidance of overcrowding or excessive spacing between objects. The C2C loss enhances the learning of spatial relationships. By comparing row 1 and row 4 in Tab. VII, the object spacing (D_{obj} 0.452 \rightarrow 0.215) is better regulated. Combining all three hierarchical relationship losses achieves the best values on all metrics.

TABLE VII: Ablation study on the relationship losses.

O2R	O2O	C2C	FID↓	KID $\times 0.001$ ↓	SCA	CKL $\times 0.01$ ↓	Col _{obj} ↓	Col _{scene} ↓	D _{obj} ↓
			51.462	3.925	0.579	0.273	0.254	0.762	0.452
✓			46.469	1.119	0.519	0.238	0.168	0.555	0.292
	✓		45.564	0.868	0.495	0.151	0.140	0.460	0.218
		✓	45.722	0.862	0.507	0.208	0.156	0.523	0.215
✓	✓	✓	44.566	0.711	0.496	0.125	0.135	0.449	0.206

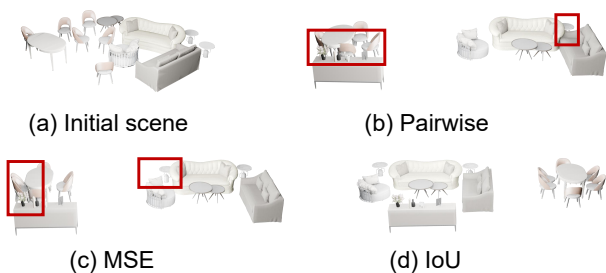


Fig. 11: Comparative visualization of same-scene rearrangement with different relationship-modeling regularizations. The red boxes highlight incorrect furniture placements.

Alternatives to the IoU-based Relationship Losses. We validate the IoU-based loss against two other alternatives: 1) pairwise distance-based loss, which minimizes the pairwise

distance variation between two objects in the triplet when comparing predictions with the ground truth (GT); 2) rendering the triplets and calculating the pixel-level mean squared error (MSE). The visualization results of scene rearrangement using different losses are shown in Fig. 11. The results in Tab. V demonstrate that the best performance is achieved by calculating the IoU-based loss.

F. Analysis and Discussions

Rotation and Translation Invariance. We first validate whether rotation invariance can improve the results when comparing the predicted object triplet and the corresponding GT object triplet. For the rotation invariance setting, we first align the edge with the same semantic labels and the longest length from the two comparing triplets, and then calculate the IoU loss. As shown in Tab. VIII, introducing rotation invariance yields no performance improvement.

Regarding translation invariance, we compared two triplet configurations: one centered at the origin (introducing translation invariance) and one without centering (removing translation invariance). Results in Tab. VIII demonstrate that incorporating translation invariance improves performance.

TABLE VIII: The impact of translation and rotation invariance on the performance.

Invariance	FID↓	KID $\times 0.001$ ↓	SCA	CKL $\times 0.01$ ↓	Col _{obj} ↓	Col _{scene} ↓	D _{obj} ↓
None	46.291	1.466	0.511	0.213	0.159	0.531	0.219
Rotation	47.136	1.423	0.512	0.213	0.162	0.535	0.228
Translation	44.566	0.711	0.496	0.125	0.135	0.449	0.206

Weights for Loss Functions. We validate the balancing weights for O2O, O2R, and C2C relationships with respect to the D_{obj} and Col_{obj} metrics. For the O2R loss, Fig. 13 (a) shows that 0.025 yields the best overall metrics. Conversely, excessively high (e.g., 0.045) or low (e.g., 0.005) weights lead to worse D_{obj} and Col_{obj} values. Fig. 13 (b) demonstrates that both D_{obj} and Col_{obj} are optimal when the weight of O2O losses is approximately 0.05. Fig. 13 (c) shows that the optimal results are achieved when the weight of the C2C loss is approximately 0.04.

G. Use Cases and Applications

Fig. 12 presents an end-to-end workflow that takes as input a floorplan (a) and a set of furniture objects to generate an indoor layout (b). Subsequently, additional specified objects

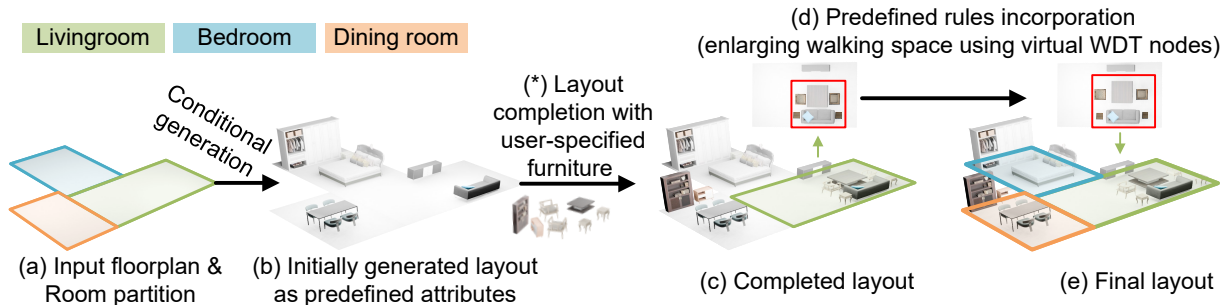


Fig. 12: A workflow example for layout generation and editing with predefined attributes and rules.

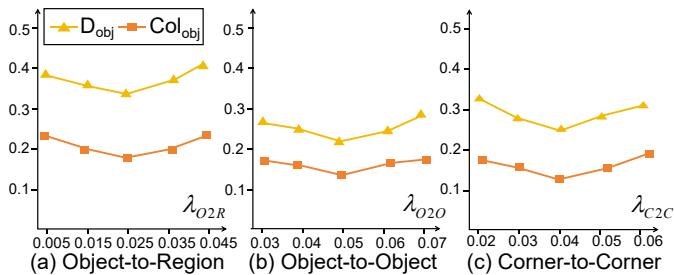


Fig. 13: Evaluations on the varying weights for loss balancing.

are integrated into the initial scene to produce a coherent interior arrangement (c). To satisfy user-defined spacing requirements, the system incorporates spatial relationships and utilizes WDT nodes to automatically adjust furniture positions (d), thereby yielding a finalised layout that adheres to design specifications (e). The resulting output is a customised design solution that both respects user input and complies with predefined spatial relationships. Accordingly, this framework enables spatial relationship-aware layout generation while also supporting flexible, user-in-the-loop refinement.

H. Limitations

While HierRelTriple demonstrates promising results in generating indoor layouts with better spatial relationships, there are still several limitations that need to be addressed. The method employs 3D bounding boxes to abstract away the geometric details of objects. However, real-world furniture often exhibits irregular shapes—for example, the sofa illustrated in Fig. 14 (a) is positioned far from the coffee table. The lack of explicit constraints between functional regions may result in generated objects intersecting with one another, as demonstrated in Fig. 14 (b). An additional core challenge is the difficulty of learning 3D spatial relationships with bounding box-based object abstractions, which leads to unnecessary ambiguity and inaccuracies. For instance, a table and a chair can be well-separated in the 3D space but usually have overlaps when using 3D bounding box-based representations. Therefore, it is interesting to explore more fine-grained 3D abstractions that can better reflect 3D layouts without the bother of too many shape details. Additionally, existing indoor datasets are significantly simpler than real-world scenes, both in terms of object diversity and layout complexity. Constructing large-scale layouts that include a

wide variety of scenes, from residential to commercial spaces, will facilitate more realistic layout modeling.



Fig. 14: Cases of failure. We present representative failure cases of our scene generation results. The erroneous regions are highlighted with red boxes.

V. CONCLUSION

In this paper, we introduced HierRelTriple, a novel framework for furniture layout generation. We leverage the indoor hierarchy to automatically extract object-to-region, object-to-object and corner-to-corner relationships and integrate the learning of these relationships into a generative diffusion framework. Our method aims to ensure realistic and functional layouts that respect practical relationships. Experimental results demonstrate that HierRelTriple outperforms existing methods in a wide variety of metrics. Future work will explore adapting the hierarchical relational paradigm to multi-room or mixed-use environments to broaden its applicability and enable comprehensive, data-driven solutions for complex interior designs.

REFERENCES

- [1] R. M. Smelik, T. Tutenel, R. Bidarra, and B. Benes, “A survey on procedural modelling for virtual worlds,” in *Computer graphics forum*, vol. 33, no. 6. Wiley Online Library, 2014, pp. 31–50.
- [2] C. Ma, O. Guerra-Santin, and M. Mohammadi, “Smart home modification design strategies for ageing in place: a systematic review,” *Journal of Housing and the Built Environment*, vol. 37, no. 2, pp. 625–651, 2022.
- [3] D. Fernandez-Chaves, J.-R. Ruiz-Sarmiento, A. Jaenal, N. Petkov, and J. Gonzalez-Jimenez, “Robot@ virtualhome, an ecosystem of virtual environments and tools for realistic indoor robotic simulation,” *Expert Systems with Applications*, vol. 208, p. 117970, 2022.
- [4] M. Fisher, D. Ritchie, M. Savva, T. Funkhouser, and P. Hanrahan, “Example-based synthesis of 3d object arrangements,” *ACM Transactions on Graphics (TOG)*, vol. 31, no. 6, pp. 1–11, 2012.
- [5] S.-K. Zhang, H. Tam, Y.-X. Li, T.-J. Mu, and S.-H. Zhang, “Sceneviewer: Automating residential photography in virtual environments,” *IEEE Transactions on Visualization and Computer Graphics*, vol. 29, no. 12, pp. 5523–5537, 2022.
- [6] Q. Fu, S. He, X. Li, and H. Fu, “Plannet: a generative model for component-based plan synthesis,” *IEEE Transactions on Visualization and Computer Graphics*, vol. 30, no. 8, pp. 4739–4751, 2023.

- [7] X. Wang, C. Yeshwanth, and M. Nießner, “Sceneformer: Indoor scene generation with transformers,” in *2021 International Conference on 3D Vision (3DV)*. IEEE, 2021, pp. 106–115.
- [8] D. Paschalidou, A. Kar, M. Shugrina, K. Kreis, A. Geiger, and S. Fidler, “Atiss: Autoregressive transformers for indoor scene synthesis,” *Advances in Neural Information Processing Systems*, vol. 34, pp. 12 013–12 026, 2021.
- [9] Q. A. Wei, S. Ding, J. J. Park, R. Sajjani, A. Poulenard, S. Sridhar, and L. Guibas, “Lego-net: Learning regular rearrangements of objects in rooms,” in *Proceedings of the IEEE/CVF Conference on Computer Vision and Pattern Recognition*, 2023, pp. 19 037–19 047.
- [10] L. Maillard, N. Sereyjal-Garros, T. Durand, and M. Ovsjanikov, “Debara: Denoising-based 3d room arrangement generation,” *Advances in Neural Information Processing Systems*, vol. 37, pp. 109 202–109 232, 2024.
- [11] J. Tang, Y. Nie, L. Markhasin, A. Dai, J. Thies, and M. Nießner, “Diffuscene: Denoising diffusion models for generative indoor scene synthesis,” in *Proceedings of the IEEE/CVF conference on computer vision and pattern recognition*, 2024, pp. 20 507–20 518.
- [12] Y. Yang, B. Jia, P. Zhi, and S. Huang, “Physcene: Physically interactable 3d scene synthesis for embodied ai,” in *Proceedings of the IEEE/CVF Conference on Computer Vision and Pattern Recognition*, 2024, pp. 16 262–16 272.
- [13] J.-M. Sun, J. Yang, K. Mo, Y.-K. Lai, L. Guibas, and L. Gao, “Haisor: Human-aware indoor scene optimization via deep reinforcement learning,” *ACM Transactions on Graphics*, vol. 43, no. 2, pp. 1–17, 2024.
- [14] K. Leimer, P. Guerrero, T. Weiss, and P. Musialski, “Layoutenhancer: Generating good indoor layouts from imperfect data,” in *SIGGRAPH Asia 2022 Conference Papers*, 2022, pp. 1–8.
- [15] X. Hong, H. Yi, F. He, and Q. Cao, “Human-aware 3d scene generation with spatially-constrained diffusion models,” *arXiv preprint arXiv:2406.18159*, 2024.
- [16] Q. Sun, H. Zhou, W. Zhou, L. Li, and H. Li, “Forest2seq: Revitalizing order prior for sequential indoor scene synthesis,” in *European Conference on Computer Vision*. Springer, 2024, pp. 251–268.
- [17] A. Lange, “The woman who invented the kitchen,” *Slate Magazine*. Retrieved, vol. 592, p. 2, 2012.
- [18] P. Dhariwal and A. Nichol, “Diffusion models beat gans on image synthesis,” *Advances in neural information processing systems*, vol. 34, pp. 8780–8794, 2021.
- [19] A. Ramesh, M. Pavlov, G. Goh, S. Gray, C. Voss, A. Radford, M. Chen, and I. Sutskever, “Zero-shot text-to-image generation,” in *International conference on machine learning*. Pmlr, 2021, pp. 8821–8831.
- [20] R. Rombach, A. Blattmann, D. Lorenz, P. Esser, and B. Ommer, “High-resolution image synthesis with latent diffusion models,” in *Proceedings of the IEEE/CVF conference on computer vision and pattern recognition*, 2022, pp. 10 684–10 695.
- [21] A. Luo, Z. Zhang, J. Wu, and J. B. Tenenbaum, “End-to-end optimization of scene layout,” in *Proceedings of the IEEE/CVF Conference on Computer Vision and Pattern Recognition*, 2020, pp. 3754–3763.
- [22] L. Gao, J.-M. Sun, K. Mo, Y.-K. Lai, L. J. Guibas, and J. Yang, “Scenehn: Hierarchical graph networks for 3d indoor scene generation with fine-grained geometry,” *IEEE Transactions on Pattern Analysis and Machine Intelligence*, vol. 45, no. 7, pp. 8902–8919, 2023.
- [23] G. Zhai, E. P. Örnek, S.-C. Wu, Y. Di, F. Tombari, N. Navab, and B. Busam, “Commonscenes: Generating commonsense 3d indoor scenes with scene graph diffusion,” *Advances in Neural Information Processing Systems*, vol. 36, pp. 30 026–30 038, 2023.
- [24] M.-J. Yang, Y.-X. Guo, B. Zhou, and X. Tong, “Indoor scene generation from a collection of semantic-segmented depth images,” in *Proceedings of the IEEE/CVF International Conference on Computer Vision*, 2021, pp. 15 203–15 212.
- [25] J. Y. Koh, H. Agrawal, D. Batra, R. Tucker, A. Waters, H. Lee, Y. Yang, J. Baldridge, and P. Anderson, “Simple and effective synthesis of indoor 3d scenes,” in *Proceedings of the AAAI Conference on Artificial Intelligence*, vol. 37, no. 1, 2023, pp. 1169–1178.
- [26] S. Bahmani, J. J. Park, D. Paschalidou, X. Yan, G. Wetzstein, L. Guibas, and A. Tagliasacchi, “Cc3d: Layout-conditioned generation of compositional 3d scenes,” in *Proceedings of the IEEE/CVF International Conference on Computer Vision*, 2023, pp. 7171–7181.
- [27] Y. Xu, M. Chai, Z. Shi, S. Peng, I. Skorokhodov, A. Siarohin, C. Yang, Y. Shen, H.-Y. Lee, B. Zhou *et al.*, “Discoscene: Spatially disentangled generative radiance fields for controllable 3d-aware scene synthesis,” in *Proceedings of the IEEE/CVF conference on computer vision and pattern recognition*, 2023, pp. 4402–4412.
- [28] D. Ritchie, K. Wang, and Y.-a. Lin, “Fast and flexible indoor scene synthesis via deep convolutional generative models,” in *Proceedings of the IEEE/CVF conference on computer vision and pattern recognition*, 2019, pp. 6182–6190.
- [29] K. Wang, Y.-A. Lin, B. Weissmann, M. Savva, A. X. Chang, and D. Ritchie, “Planit: Planning and instantiating indoor scenes with relation graph and spatial prior networks,” *ACM Transactions on Graphics (TOG)*, vol. 38, no. 4, pp. 1–15, 2019.
- [30] W. Para, P. Guerrero, T. Kelly, L. J. Guibas, and P. Wonka, “Generative layout modeling using constraint graphs,” in *Proceedings of the IEEE/CVF international conference on computer vision*, 2021, pp. 6690–6700.
- [31] Y. Nie, A. Dai, X. Han, and M. Nießner, “Learning 3d scene priors with 2d supervision,” in *Proceedings of the IEEE/CVF Conference on Computer Vision and Pattern Recognition*, 2023, pp. 792–802.
- [32] M. Lewis, Y. Liu, N. Goyal, M. Ghazvininejad, A. Mohamed, O. Levy, V. Stoyanov, and L. Zettlemoyer, “Bart: Denoising sequence-to-sequence pre-training for natural language generation, translation, and comprehension,” *arXiv preprint arXiv:1910.13461*, 2019.
- [33] C. Lin and Y. Mu, “Instructscene: Instruction-driven 3d indoor scene synthesis with semantic graph prior,” in *The Twelfth International Conference on Learning Representations*, 2024.
- [34] G. Zhai, E. P. Örnek, D. Z. Chen, R. Liao, Y. Di, N. Navab, F. Tombari, and B. Busam, “Echoscene: Indoor scene generation via information echo over scene graph diffusion,” in *European Conference on Computer Vision*. Springer, 2024, pp. 167–184.
- [35] Z. Yang, K. Lu, C. Zhang, J. Qi, H. Jiang, R. Ma, S. Yin, Y. Xu, M. Xing, Z. Xiao, J. Long, X. Liu, and G. Zhai, “Mmgdreamer: Mixed-modality graph for geometry-controllable 3d indoor scene generation,” in *AAAI Conference on Artificial Intelligence*, 2025. [Online]. Available: <https://api.semanticscholar.org/CorpusID:276249862>
- [36] R. Fu, Z. Wen, Z. Liu, and S. Sridhar, “Anyhome: Open-vocabulary generation of structured and textured 3d homes,” in *European Conference on Computer Vision*. Springer, 2024, pp. 52–70.
- [37] A. cCelen, G. Han, K. Schindler, L. van Gool, I. Armeni, A. Obukhov, and X. Wang, “I-design: Personalized llm interior designer,” in *ECCV Workshops*, 2024. [Online]. Available: <https://api.semanticscholar.org/CorpusID:268876421>
- [38] W. Feng, W. Zhu, T.-j. Fu, V. Jampani, A. Akula, X. He, S. Basu, X. E. Wang, and W. Y. Wang, “Layoutgpt: Compositional visual planning and generation with large language models,” *Advances in Neural Information Processing Systems*, vol. 36, pp. 18 225–18 250, 2023.
- [39] Y. Yang, J. Lu, Z. Zhao, Z. Luo, J. J. Yu, V. Sanchez, and F. Zheng, “Llplace: The 3d indoor scene layout generation and editing via large language model,” *arXiv preprint arXiv:2406.03866*, 2024.
- [40] Y. Ding, X. Zhang, C. Paxton, and S. Zhang, “Task and motion planning with large language models for object rearrangement,” in *2023 IEEE/RSJ International Conference on Intelligent Robots and Systems (IROS)*. IEEE, 2023, pp. 2086–2092.
- [41] H. I. I. Tam, H. I. D. Pun, A. T. Wang, A. X. Chang, and M. Savva, “SceneMotifCoder: Example-driven Visual Program Learning for Generating 3D Object Arrangements,” in *Proceedings of the IEEE Conference on 3D Vision (3DV)*, 2025.
- [42] C. Wang, H. Zhong, M. Chai, M. He, D. Chen, and J. Liao, “Chat2layout: Interactive 3d furniture layout with a multimodal llm,” *arXiv preprint arXiv:2407.21333*, 2024.
- [43] J. De Chiara, J. Panero, and M. Zelnik, *Time-saver standards for interior design and space planning*. McGraw-Hill, 2001.
- [44] H. Dharmo, F. Manhardt, N. Navab, and F. Tombari, “Graph-to-3d: End-to-end generation and manipulation of 3d scenes using scene graphs,” in *Proceedings of the IEEE/CVF International Conference on Computer Vision*, 2021, pp. 16 352–16 361.
- [45] R. Xu, L. Hui, Y. Han, J. Qian, and J. Xie, “Scene graph masked variational autoencoders for 3d scene generation,” in *Proceedings of the 31st ACM International Conference on Multimedia*, 2023, pp. 5725–5733.
- [46] Y. Wei, M. R. Min, G. Vosselman, L. E. Li, and M. Y. Yang, “Compositional 3d scene synthesis with scene graph guided layout-shape generation,” 2024.
- [47] M. Li, A. G. Patil, K. Xu, S. Chaudhuri, O. Khan, A. Shamir, C. Tu, B. Chen, D. Cohen-Or, and H. Zhang, “Grains: Generative recursive autoencoders for indoor scenes,” *ACM Transactions on Graphics (TOG)*, vol. 38, no. 2, pp. 1–16, 2019.
- [48] A. Chattopadhyay, X. Zhang, D. P. Wipf, H. Arora, and R. Vidal, “Learning graph variational autoencoders with constraints and structured priors for conditional indoor 3d scene generation,” in *Proceedings of the IEEE/CVF winter conference on applications of computer vision*, 2023, pp. 785–794.

- [49] S.-K. Zhang, J.-H. Liu, J. Huang, Z.-W. Chi, H. Tam, Y.-L. Yang, and S.-H. Zhang, "Sceneexplorer: An interactive system for expanding, scheduling, and organizing transformable layouts," *IEEE Transactions on Visualization and Computer Graphics*, 2024.
- [50] T. Bai, W. Bai, D. Chen, T. Wu, M. Li, and R. Ma, "Freescene: Mixed graph diffusion for 3d scene synthesis from free prompts," in *Proceedings of the Computer Vision and Pattern Recognition Conference*, 2025, pp. 5893–5903.
- [51] P. Merrell, E. Schkufza, Z. Li, M. Agrawala, and V. Koltun, "Interactive furniture layout using interior design guidelines," *ACM transactions on graphics (TOG)*, vol. 30, no. 4, pp. 1–10, 2011.
- [52] Y.-T. Yeh, L. Yang, M. Watson, N. D. Goodman, and P. Hanrahan, "Synthesizing open worlds with constraints using locally annealed reversible jump mcmc," *ACM Transactions on Graphics (TOG)*, vol. 31, no. 4, pp. 1–11, 2012.
- [53] L. F. Yu, S. K. Yeung, C. K. Tang, D. Terzopoulos, T. F. Chan, and S. J. Osher, "Make it home: automatic optimization of furniture arrangement," *ACM Transactions on Graphics (TOG)-Proceedings of ACM SIGGRAPH 2011*, v. 30,(4), July 2011, article no. 86, vol. 30, no. 4, 2011.
- [54] T. Weiss, A. Litteneker, N. Duncan, M. Nakada, C. Jiang, L.-F. Yu, and D. Terzopoulos, "Fast and scalable position-based layout synthesis," *IEEE Transactions on Visualization and Computer Graphics*, vol. 25, no. 12, pp. 3231–3243, 2018.
- [55] S.-H. Zhang, S.-K. Zhang, W.-Y. Xie, C.-Y. Luo, Y.-L. Yang, and H. Fu, "Fast 3d indoor scene synthesis by learning spatial relation priors of objects," *IEEE Transactions on Visualization and Computer Graphics*, vol. 28, no. 9, pp. 3082–3092, 2021.
- [56] S.-K. Zhang, H. Tam, Y. Li, K.-X. Ren, H. Fu, and S.-H. Zhang, "Scenedirector: Interactive scene synthesis by simultaneously editing multiple objects in real-time," *IEEE Transactions on Visualization and Computer Graphics*, vol. 30, no. 8, pp. 4558–4569, 2023.
- [57] X. Hong, H. Yi, F. He, and Q. Cao, "Human-aware 3d scene generation with spatially-constrained diffusion models," *ArXiv*, vol. abs/2406.18159, 2024. [Online]. Available: <https://api.semanticscholar.org/CorpusID:270737886>
- [58] A. Vaswani, N. Shazeer, N. Parmar, J. Uszkoreit, L. Jones, A. N. Gomez, Ł. Kaiser, and I. Polosukhin, "Attention is all you need," *Advances in neural information processing systems*, vol. 30, 2017.
- [59] M. Ester, H.-P. Kriegel, J. Sander, X. Xu *et al.*, "A density-based algorithm for discovering clusters in large spatial databases with noise," in *kdd*, vol. 96, no. 34, 1996, pp. 226–231.
- [60] H. Rezatofghi, N. Tsoi, J. Gwak, A. Sadeghian, I. Reid, and S. Savarese, "Generalized intersection over union: A metric and a loss for bounding box regression," in *Proceedings of the IEEE/CVF conference on computer vision and pattern recognition*, 2019, pp. 658–666.
- [61] C. D. Wickens and C. M. Carswell, "The proximity compatibility principle: Its psychological foundation and relevance to display design," *Human factors*, vol. 37, no. 3, pp. 473–494, 1995.
- [62] F. d. Goes, P. Memari, P. Mullen, and M. Desbrun, "Weighted triangulations for geometry processing," *ACM Transactions on Graphics (TOG)*, vol. 33, no. 3, pp. 1–13, 2014.
- [63] L. P. Chew, "Constrained delaunay triangulations," in *Proceedings of the third annual symposium on Computational geometry*, 1987, pp. 215–222.
- [64] H. Fu, B. Cai, L. Gao, L.-X. Zhang, J. Wang, C. Li, Q. Zeng, C. Sun, R. Jia, B. Zhao *et al.*, "3d-front: 3d furnished rooms with layouts and semantics," in *Proceedings of the IEEE/CVF International Conference on Computer Vision*, 2021, pp. 10933–10942.
- [65] M. Heusel, H. Ramsauer, T. Unterthiner, B. Nessler, and S. Hochreiter, "Gans trained by a two time-scale update rule converge to a local nash equilibrium," *Advances in neural information processing systems*, vol. 30, 2017.
- [66] M. Binkowski, D. J. Sutherland, M. Arbel, and A. Gretton, "Demystifying MMD gans," in *6th International Conference on Learning Representations, ICLR 2018, Vancouver, BC, Canada, April 30 - May 3, 2018, Conference Track Proceedings*. OpenReview.net, 2018. [Online]. Available: <https://openreview.net/forum?id=r1IUzWCW>
- [67] D. W. Scott, "Multivariate density estimation, theory, practice and visualization," *The Statistician*, vol. 43, pp. 218–219, 1992. [Online]. Available: <https://api.semanticscholar.org/CorpusID:108295844>
- [68] J. Ho, A. Jain, and P. Abbeel, "Denoising diffusion probabilistic models," *Advances in neural information processing systems*, vol. 33, pp. 6840–6851, 2020.
- [69] H. Fu, R. Jia, L. Gao, M. Gong, B. Zhao, S. Maybank, and D. Tao, "3d-future: 3d furniture shape with texture," *International Journal of Computer Vision*, vol. 129, pp. 3313–3337, 2021.